Journal of Dental Sciences

Volume 21 | Issue 2 Article 35

2026

Automated assessment of peri-implant disease severity by deep learning and image processing in periapical radiographs

Yi-Cheng Mao

Chiung-An Chen

Yuan-Jin Lin

Yu-Jen Chang

Patricia Angela R. Abu

Follow this and additional works at: https://jds.ads.org.tw/journal

Recommended Citation
Mao, Yi-Cheng; Chen, Chiung-An; Lin, Yuan-Jin; Chang, Yu-Jen; and Abu, Patricia Angela R. (2026) "Automated assessment of peri-implant disease severity by deep learning and image processing in periapical radiographs," *Journal of Dental Sciences*: Vol. 21: Iss. 2, Article 35.
Available at: https://jds.ads.org.tw/journal/vol21/iss2/35

This Original Article is brought to you for free and open access by Journal of Dental Sciences. It has been accepted for inclusion in Journal of Dental Sciences by an authorized editor of Journal of Dental Sciences. For more information, please contact cpchiang@ntu.edu.tw.

Available online at https://jds.ads.org.tw/journal/

Digital Commons

journal homepage: https://jds.ads.org.tw/journal/

Original Article

Automated assessment of peri-implant disease severity by deep learning and image processing in periapical radiographs

Yi-Cheng Mao [a], Chiung-An Chen [b*], Yuan-Jin Lin [c], Yu-Jen Chang [d], Sung-Tsun Wei [d], Shih-Lun Chen [d], Tsung-Yi Chen [e], Kuo-Chen Li [f], Wei-Chen Tu [c,g], Patricia Angela R. Abu [h]

[a] *Department of Operative Dentistry, Taoyuan Chang Gang Memorial Hospital, Taoyuan, Taiwan*
[b] *Department of Electrical Engineering, Ming Chi University of Technology, New Taipei, Taiwan*
[c] *Program on Semiconductor Manufacturing Technology, Academy of Innovative Semiconductor and Sustainable Manufacturing, National Cheng Kung University, Tainan, Taiwan*
[d] *Department of Electronic Engineering, Chung Yuan Christian University, Taoyuan, Taiwan*
[e] *Department of Electronic Engineering, Feng Chia University, Taichung, Taiwan*
[f] *Department of Information Management, Chung Yuan Christian University, Taoyuan, Taiwan*
[g] *Department of Electrical Engineering, National Cheng Kung University, Tainan, Taiwan*
[h] *Ateneo Laboratory for Intelligent Visual Environments, Department of Information Systems and Computer Science, Ateneo de Manila University, Quezon, Philippines*

Received 25 July 2025; Final revision received 6 August 2025
Available online 1 April 2026

KEYWORDS
Deep learning;
Dental radiography;
Image processing;
Peri-implantitis severity

Abstract *Background/purpose:* Dental implant surgery had become a standard treatment option for oral rehabilitation. The severity of peri-implant bone loss was a critical clinical indicator for evaluating the success of dental implants. This study assessed an automated framework combining deep learning and image processing techniques for classifying the severity of peri-implant bone loss using periapical radiographs and providing diagnostic assistance.
Materials and methods: A total of 780 periapical radiographs containing 1210 implants were analyzed. A YOLO-based object detection model was employed to localize peri-implant regions accurately. Subsequently, we applied our custom-developed peri-implant image processing pipeline and alveolar crest localization algorithm to categorize each implant into one of three severity levels. The clinical feasibility of the proposed framework was also evaluated.

* Corresponding author. Department of Electrical Engineering, Ming Chi University of Technology, 84 Gungjuan Rd, New Taipei City, 243303, Taiwan.
E-mail address: joannechen@mail.mcut.edu.tw (C.-A. Chen).

https://doi.org/10.1016/j.jds.2025.08.015
1991-7902/© 2026 Association for Dental Sciences of the Republic of China. Publishing services by Digital Commons. This is an open access article under the CC BY-NC-ND license (http://creativecommons.org/licenses/by-nc-nd/4.0/).

Results: On a test dataset of 120 periapical radiographs, the YOLOv8-S model achieved a detection precision of 98.1 %, with a sensitivity of 96.0 % and a specificity of 99.1 %. For the three-grade classification of peri-implant bone loss severity, the highest accuracy reached 96.61 %, with an overall classification accuracy of 95.8 %. In clinical feasibility testing, our framework demonstrated a 36-fold improvement in assessment speed and approximately a 7.5 % increase in diagnostic accuracy compared to manual evaluation by dental experts.
Conclusion: The proposed automated framework for assessing peri-implant bone loss severity in periapical radiographs shows strong potential to assist clinical dental practices. It is a reliable second opinion to support clinical decision-making and improve diagnostic efficiency.
© 2026 Association for Dental Sciences of the Republic of China. Publishing services by Digital Commons. This is an open access article under the CC BY-NC-ND license (http://creativecommons.org/licenses/by-nc-nd/4.0/).

Introduction

Peri-implantitis was a prevalent and clinically significant complication associated with dental implants, primarily characterized by inflammation of the alveolar bone surrounding the implant, often accompanied by progressive bone loss.[1] This condition could ultimately lead to implant failure. Epidemiological studies reported a wide range of prevalence rates, from 1.1 % to 85.0 %, depending on regional disparities in healthcare resources, underscoring the clinical importance of peri-implantitis in dental practice.[2] Traditionally, its diagnosis relied on periapical radiographic evaluation and probing depth measurements.[3] However, these methods were highly dependent on clinicians' subjective interpretation, which could lead to inter-examiner variability.[4,5] To standardize diagnosis, the American Academy of Periodontology and the European Federation of Periodontology jointly proposed a new classification system in 2018 based on staging and grading to stratify disease severity.[6] Nevertheless, the complexity of this classification limited its practical adoption in routine clinical settings, highlighting the urgent need for more efficient and objective diagnostic tools in modern dentistry.[7]

Dental imaging techniques, such as dental panoramic radiographs (DPRs) and periapical radiographs (PAs), were practical tools for identifying and classifying dental implants. However, interpreting these images typically relied on clinicians' subjective judgment, which led to variability in diagnostic outcomes.[8,9] With the rapid advancement of artificial intelligence (AI), AI-assisted interpretation in dental radiology became an increasingly necessary component of clinical practice. It was demonstrated to be well-suited for dental image analysis.[10—12] Among these approaches, convolutional neural networks (CNNs) were extensively studied and were shown to significantly improve diagnostic accuracy, enhance clinical workflow, and support decision-making across various medical applications. In implant assessment, these AI-based techniques achieved promising results in tasks such as implant identification, brand classification, and detection of peri-implantitis, often attaining over 88 % accuracy in clinical diagnostic support.[13—16]

Several recent studies had demonstrated that experienced, board-certified radiologists achieved improved diagnostic accuracy and efficiency with reduced reading times when supported by deep learning (DL) and image classification algorithms, without compromising detection or classification performance.[17,18] However, no existing studies had established the clinical efficacy of DL-based image processing in assisting dental professionals with the severity grading of peri-implantitis. Only a few studies had explored the use of DL techniques to detect the presence of peri-implantitis.[19,20] Therefore, the objective of this study was to evaluate the feasibility of using artificial intelligence combined with image processing to assist in diagnosing and classifying peri-implantitis-associated bone defects on periapical radiographs, with a particular focus on grading the severity of peri-implantitis.

Materials and methods

PA dataset collection and annotation

The dataset was provided by Chang Gung Medical Center in Taoyuan, Taiwan. 780 anonymized PAs were collected from seven Chang Gung healthcare system branches. The study protocol was approved by the Institutional Review Board of Chang Gung Medical Foundation (IRB number: 202500009B0), with informed consent waived. The inclusion criteria for PAs in this study excluded patients with a medical history of human immunodeficiency virus positivity to avoid potential confounding factors. All PAs were acquired using a high-frequency X-ray generator set to provide constant high voltage. The exposure time was incrementally adjustable from 0.03 to 3.2 s depending on clinical needs. Digital sensors with a size of 31.3 $\times$ 44.5 mm, and the image resolution was either 825 $\times$ 1200 or 820 $\times$ 562 pixels, saved in DCI format. The image development time was $\leq$5 s. In addition, an X-ray indicator ring and a sensor holder were used for all subjects to standardize the angle between the X-ray cone and the sensor, thereby reducing variability in image geometry.

PAs were chosen because they provide a standardized visualization of implant structures with minimal distortion. PAs are the most reliable method for capturing the entire tooth and implant from crown to apex, making them suitable for assessing peri-implant bone levels.[21] The PAs were

annotated independently by five oral experts with over five years of clinical experience. Each expert annotated the PAs individually without influence from others. Final annotations for each PA were determined by majority voting to ensure reliability and consistency. Based on the annotation results, 1210 implant teeth were identified across the 780 PAs. From the dataset, 120 PAs were reserved as the test set, while the remaining were split into training and validation sets using a 75 %–25 % ratio. The test dataset was strictly excluded from the training process to ensure the credibility of the clinical evaluation. The development, training, and validation of the deep learning models were conducted under the supervision of senior researchers with extensive experience. A blinded protocol was implemented throughout the validation and testing phases to eliminate operator bias.

Peri-implant bone loss severity evaluation method

Peri-implantitis was typically classified by the severity of bone loss, which is measured based on the vertical distance from the alveolar crest (ALC) to the most apical point of bone-to-implant contact.[22–25] We quantified implant length using the number of implant threads and evaluated the severity of bone loss by calculating the proportion of exposed threads. Based on this ratio, peri-implantitis was categorized into three severity grades: Grade A was defined as no bone loss with bone loss-to-age percentage less than 25 %; Grade B indicated moderate bone loss with 25 % to less than 50 % loss; and Grade C represented severe bone loss with 50 % or more. The peri-implant severity assessment formula was shown in (1).

$$\text{Bone loss} = (\text{ALC located at the xth implant thread} / \text{Total number of implant threads}) \times 100\% \quad (1)$$

Automated peri-implant detection using YOLO architecture

This study employed a YOLO-based object detection architecture for peri-implant detection in PA. We used YOLOv8 as the core model and trained it on 660 PA for validation. The YOLOv8 framework was illustrated in Fig. 1

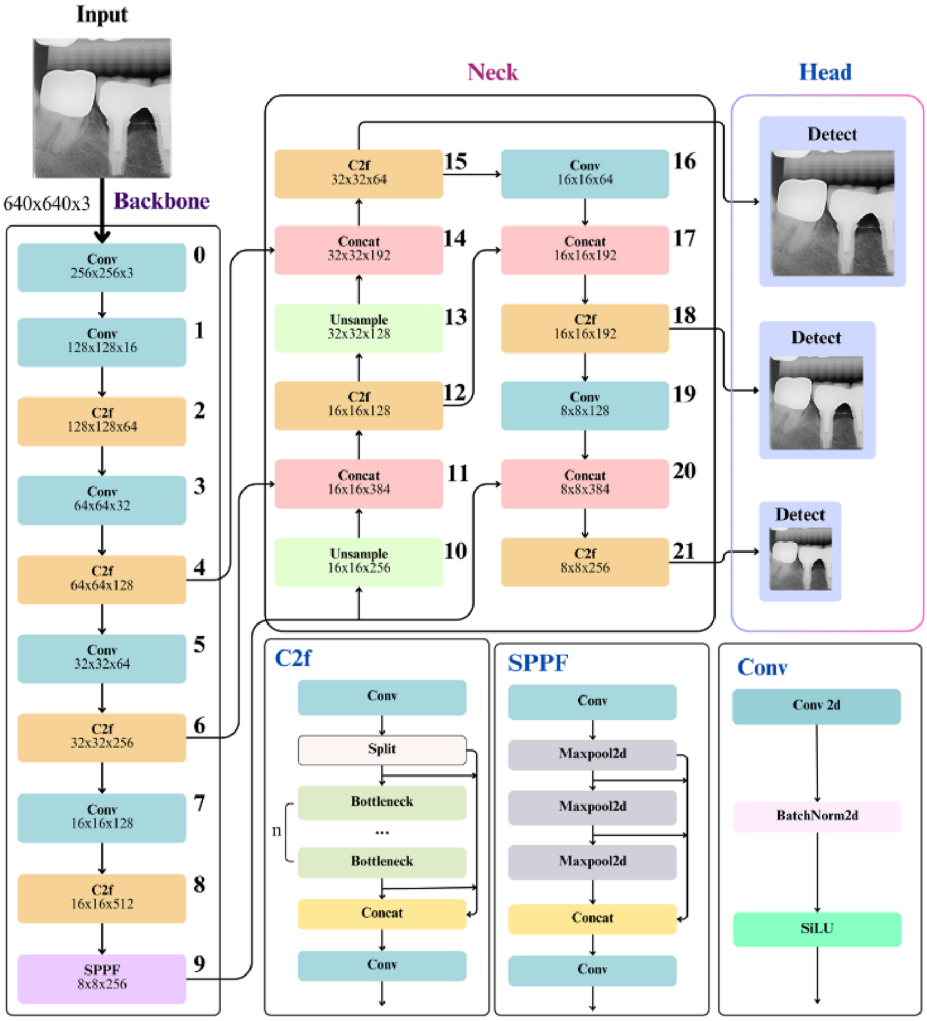

Figure 1 The YOLOv8 object detection model performs multi-scale feature extraction, aggregation, and prediction, enabling robust detection of peri-implant regions in periapical radiograph.

and was developed by Ultralytics (Ultralytics, San Francisco, CA, USA). Each PA input into YOLOv8 first passed through the Backbone module, where the Cross-Stage Partial Darknet-53 (CSPDarknet53) served as the feature extraction backbone. During this stage, the model automatically learned multi-level visual features such as edges, shapes, and densities from the raw image. The extracted features were fed into the Neck module, specifically a Path Aggregation Network (PANet), which fused feature maps at different scales. This enhanced the model's ability to detect implants of varying sizes by integrating both large- and small-scale features. Finally, the Head module processed these aggregated feature maps to generate predictions, including bounding box coordinates, category classification (e.g., peri-implant or background), and associated confidence scores for each detected object. After applying non-maximum suppression (NMS) to eliminate redundant bounding boxes, the model outputs the spatial locations and confidence scores of all detected implants in each PA image. These results were the foundation for subsequent bone loss quantification and severity classification.

Peri-implant pre-processing

Image preprocessing was critical in determining the severity of peri-implant conditions based on implant threads. First, the original input image (Fig. 2A) was converted into a single-channel grayscale image (Fig. 2B) to simplify the subsequent processing and enhance the visibility of the implant thread edges. Then, Contrast Limited Adaptive Histogram Equalization (CLAHE) was applied to improve the visibility and clarity of the implant threads (Fig. 2C). To further reduce granular noise while preserving the thread structure, non-local means filtering was applied to the enhanced image (Fig. 2C), resulting in a denoised image (Fig. 2D), and a binarization technique was used to retain the implant and remove the background (Fig. 2E).

Furthermore, variations in the imaging angle of each periapical radiograph resulted in different tilting orientations of the peri-implant regions detected by YOLO, which posed challenges for accurately locating implant threads. To address this issue, Algorithm 1 was employed to normalize the tilt of each peri-implant region, aligning it to approximately 0° relative to the horizontal axis. The algorithm first identified all possible contours in Fig. 2E and selected the one with the largest enclosed area as the implant region. It then inferred the direction of the major axis using the minimum bounding rectangle and calculated the original rotation angle $\theta_{Original}$ (ranging from 90° to 0°), which was shown in Fig. 2F. If the arctangent of $\theta_{Original}$ was less than 45°, indicating that the major axis was closer to vertical, an additional 90° was added to align the implant axis horizontally. Otherwise, the original angle was retained if the axis was already close to horizontal ($\theta_{Original} \geq 45°$). This angle adjustment mechanism ensured that the major axis of the implant threads was normalized to a horizontal orientation. The rotated image (Fig. 2G) was subsequently split horizontally into upper and lower halves (Fig. 2H), serving as the standardized input format for the subsequent thread detection algorithm.

ALC localization and implant thread annotation

This study proposed an automated framework for implant thread extraction and annotation, aimed at accurately reconstructing the contour structure of dental implant threads. By performing vertical projection analysis on the upper and lower halves of the implant image in Fig. 2H, distinct peak values in specific regions of the projection were identified, which corresponded to the endpoints of implant threads (Fig. 3A). Subsequently, using the implant contour information, local boundary feature points were extracted from designated vertical ranges at each horizontal scanning position. These points respectively represented the upper and lower edge contours of the threads. A

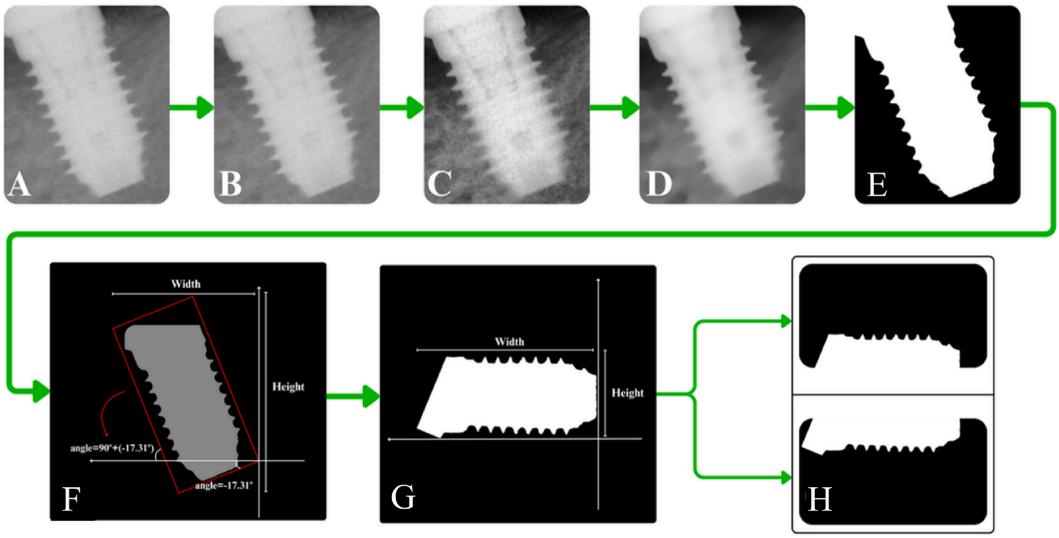

Figure 2 Peri-implant image pre-processing. (A) Original image, (B) Grayscale, (C) Contrast limited adaptive histogram equalization, (D) Non-local means filtering, (E) Binary method, (F) Rotated implant, (G) Algorithm rotated results, (H) Upper and lower implant threads.

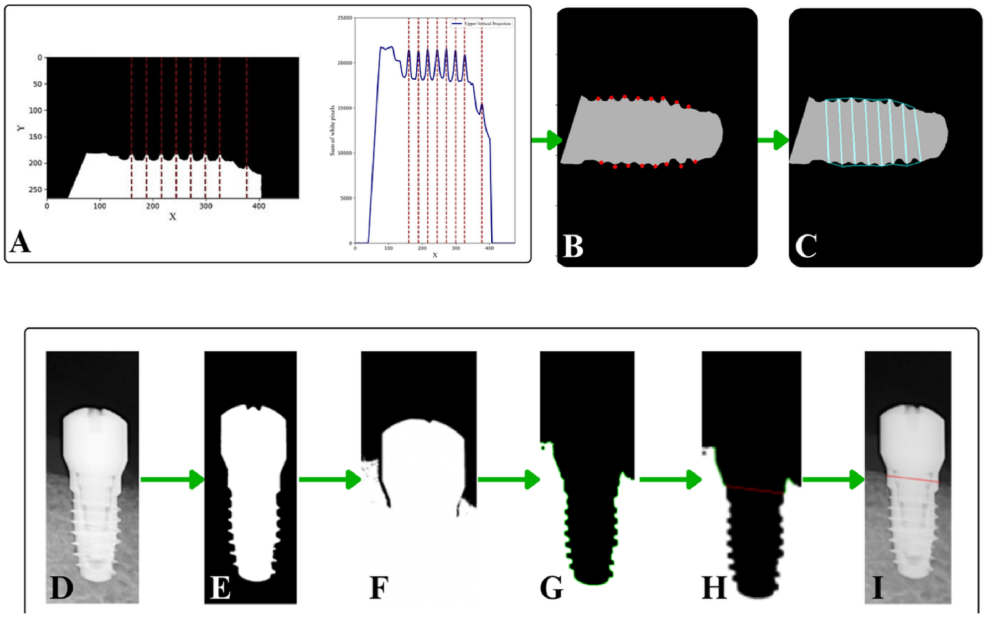

Figure 3 Implant thread annotation and ALC detection process. (A) Vertical projection of the upper implant threads, (B) Point detection, (C) Thread drawing, (D) Brightness compensation, (E) Binary, (F) Second binary, (G) Contour drawing, (H) ALC annotation, (I) Overlay onto the original image.

transparent layer matching the original image's dimensions was then created, where all detected peak positions were marked with horizontal lines, and the corresponding boundary points were annotated with circular markers (Fig. 3B). To further reconstruct the thread structure, the upper and lower boundary points were connected using smooth curves to approximate the geometric profile of the initial thread region (Fig. 3C). This reconstruction established a reference framework for the subsequent quantitative assessment of peri-implant bone loss.

The alveolar level line (ALC) was used as the reference baseline for evaluating the severity of bone loss. After the step shown in Fig. 2D, brightness compensation was applied to reduce the background intensity and enhance the visibility of the implant structure (Fig. 3D). Subsequent binarization and dilation operations were performed to obtain the binary implant mask (Fig. 3E). The original image was also binarized to generate Fig. 3F and 3G was obtained by subtracting Fig. 3E from Fig. 3F, resulting in a binary image distinguishing the gingiva and the implant. Fig. 3E then underwent a second dilation step, and subtracting this result from Fig. 3G removed the green boundary line below the implant while preserving the green edge region above the ALC. Finally, the rightmost green contour point on the left side and the leftmost green point on the right side related to a red line to form the ALC (Fig. 3H). The detected ALC line was then superimposed on the implant thread annotation result to generate the final overlay image (Fig. 3I).

Framework evaluates metrices

This study employed multiple objective evaluation metrics to assess the reliability and robustness of the proposed method for classifying peri-implant bone loss severity. These metrics were derived from four parameters obtained through the confusion matrix: true positive (T_P), true negative (T_N), false positive (F_P), and false negative (F_N). The evaluation indicators applied in this study were as follows:

1. Accuracy:The overall classification performance represents the ratio of correctly predicted instances to the total number of samples evaluated.
2. Precision:The proportion of true positive predictions among all instances predicted as positive, reflecting the model's ability to minimize false positives.
3. Sensitivity:The proportion of correctly predicted positive instances among all actual positive samples, indicating the model's capacity to capture relevant cases.
4. F1-Score:The harmonic means of precision and sensitivity, providing a balanced metric particularly effective for imbalanced class distributions.
5. mAP:The average of class-wise average precisions, widely adopted in object detection benchmarks to evaluate localization and classification accuracy across all categories.
6. 95 % Confidence Interval (95 % CI):A statistical range that estimates where the true population mean is likely to fall, with 95 % confidence. It reflects the uncertainty around the sample mean obtained from the observed data. Here, $\tilde{x}$ represented sample mean, s was the sample standard deviation, n was the sample size, $t_{a/2,df}$ was the t-score corresponding to the desired confidence level and degrees of freedom.

$$\text{Accuracy} = \frac{T_P + T_N}{T_P + T_N + F_P + F_N} \tag{2}$$

$$\text{Precision} = \frac{T_P}{T_P + F_P} \tag{3}$$

Table 1 Validation results of deep learning model for single implant thread detection.

Method	Accuracy (%) (↑)	Precision (%) (↑)	Sensitivity (%) (↑)	Specificity (%) (↑)	F1-score (%) (↑)	mAP50 (%) (↑)
YOLOv8-S	98.7	98.1	96.0	99.1	97.0	99.2
YOLOv9-S	91.4	98.1	94.6	97.8	96.3	97.1
YOLOv10-S	84.8	91.0	90.3	94.2	90.6	95.4
YOLO11-S	93.1	96.5	97.8	98.4	97.1	98.6
YOLO12-S	90.0	96.4	96.4	97.1	96.4	97.8
RF-DETR	91.5	92.1	89.8	92.8	90.9	97.3

YOLO, you only look once.
Accuracy = [true positive (T_P) + true negative (T_N)]/[true positive (T_P) + true negative (T_N) + false positive (F_P) + false negative (F_N)].
Precision = $T_P/(T_P + F_P)$.
Sensitivity(recall) = $T_P/(T_P + F_N)$.
Specificity = $T_N/(T_N + F_P)$.
F1-score = 2 × [(Precision × Sensitivity)/(Precision + Sensitivity)].
$mAP = \frac{1}{n}\sum_{i=1}^{n}(\text{average precision})_i$.
(↑) indicates that a higher value of the corresponding metric represents better model performance.

$$\text{Sensitivity} = \frac{T_P}{T_P + F_N} \quad (4)$$

$$\text{Specificity} = \frac{T_N}{T_N + F_P} \quad (5)$$

$$\text{F1 Score} = 2 \times \frac{\text{Precision} \times \text{Sensitivity}}{\text{Precision} + \text{Sensitivity}} \quad (6)$$

$$mAP = \frac{1}{n}\sum_{i=1}^{n} AP_i \quad (7)$$

$$95\%\ CI = \tilde{x} \pm t_{a/2,df} \times \frac{s}{\sqrt{n}} \quad (8)$$

Results

Table 1 presents the performance of the object detection model in identifying peri-implant regions using a test set of 120 unlabeled PA. Among the evaluated models, YOLOv8-S demonstrated the best overall performance, achieving the highest scores across several key metrics: accuracy of 98.7 % (95 % CI:97.9 %—99.1 %), precision of 98.1 % (95 % CI:97.3 %—98.7 %), F1-score of 97.0 % (95 % CI:96.8 %—98.4 %), and mAP50 of 99.2 % (95 % CI:98.8 %—99.6 %). Notably, it achieved a sensitivity of 96.0 % (95 % CI:95.7 %—98.3 %) and a specificity of 99.1 % (95 % CI:97.9—99.4 %). In real-world clinical applications, high sensitivity indicates that the system rarely misses suspected peri-implant cases, thereby facilitating early intervention and treatment. Conversely, high specificity helps reduce unnecessary clinical interventions and resource consumption, allowing clinicians to focus on cases that truly require attention.

Fig. 4A illustrated the confusion matrix results for different peri-implant severity grades on the test dataset. The diagonal elements (from top-left to bottom-right) represented the number of correctly predicted samples, showing that most validation images were accurately

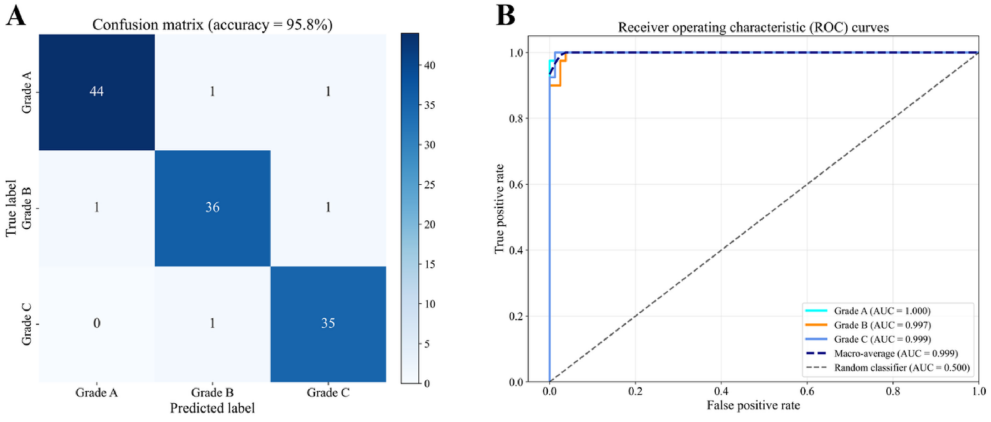

Figure 4 Peri-implant bone loss severity grades (A) confusion matrix with three types of peri-implant severity level classification result. Grade A was defined as no bone loss with bone loss-to-age percentage less than 25 %; Grade B indicated moderate bone loss with 25 % to less than 50 % loss; and Grade C represented severe bone loss with 50 % or more. (B) Receiver operating characteristic curve with different peri-implant levels.

Table 2 Evaluation results of each peri-implant severity classification.

Grade level	Accuracy (%) (↑)	Precision (%) (↑)	Sensitivity (%) (↑)	Specificity (%) (↑)	F1-score (%) (↑)	mAP50 (%) (↑)
Grade A	97.50	97.78	95.65	98.65	96.70	96.8
Grade B	96.67	94.74	94.74	97.56	94.74	96.2
Grade C	97.50	94.60	97.22	97.62	95.88	96.3

Accuracy = [true positive (TP) + true negative (TN)]/[true positive (TP) + true negative (TN) + false positive (FP) + false negative (FN)].
Precision = TP/(TP + FP).
Sensitivity(recall) = TP/(TP + FN).
Specificity = TN/(TN + FP).
F1-score = 2 × [(Precision × Sensitivity)/(Precision + Sensitivity)].
mAP = $\frac{1}{n}\sum_{i=1}^{n}(\text{average precision})_i$.
Grade A: no bone loss with bone loss percentage less than 25 %. Grade B: indicated moderate bone loss with 25 % to less than 50 % loss. Grade C: represented severe bone loss with 50 % or more.
(↑) indicates that a higher value of the corresponding metric represents better model performance.

classified, achieving an overall grading accuracy of 95.8 % (95 % CI:95.18 %–97.29 %). Table 2 further detailed the evaluation metrics for each severity level, revealing a classification accuracy of 97.50 % (95 % CI:96.91 %–98.45 %) for Grade A, 96.67 % (95 % CI:96.24 %–97.95 %) for Grade B, and 97.50 % (95 % CI:96.7 %–98.3 %) for Grade C. Fig. 4B presented the ROC curves for the three severity levels, assessing the classification performance of each grade. The Area Under the Curve (AUC) scores were 1.000 (95 % CI:98.8 %–99.9 %) for Grade A, 0.997 (95 % CI:98.3 %–99.9 %) for Grade B, and 0.999 (95 % CI:0.989–0.999) for Grade C, with an average AUC of 0.999 (95 % CI:98.5 %–99.9 %). These results further confirmed that the proposed method effectively reduced the risk of missed diagnoses in early-stage clinical screening.

Table 3 presented the clinical evaluation results comparing manual interpretation with the proposed framework. Three dental experts independently assessed the same images without mutual interference, and a senior researcher calculated the average diagnostic accuracy and interpretation time to ensure data reliability. Four images were randomly selected from each of the three severity grades for the evaluation. The results showed that the average interpretation time for manual assessment was approximately 6.625 s, whereas the proposed framework required only 0.183 s. Regarding diagnostic accuracy, the manual interpretation achieved an average of 88.82 % (95 % CI:88.63 %–95.9 %), while the proposed method attained a significantly higher accuracy of 96.39 % (95 % CI:95.97 %–98.2 %).

Discussion

Peri-implantitis is a complex and severe biological complication that requires accurate diagnosis to prevent implant failure and ensure timely, evidence-based treatment.[26] Tailored treatment plans should incorporate both non-surgical and surgical interventions, considering the morphology and severity of the bone defect to optimize clinical outcomes and prolong implant longevity. Currently, PAs are commonly used in clinical practice to assess peri-implant regions.[22] The severity of bone loss is typically estimated by visually evaluating the relative position between the implant threads and the ALC. [22–25] However, variability in image quality and unclear ALC boundaries often contribute to difficulties in diagnosis and inconsistencies caused by subjective interpretation. In clinical settings involving many implant cases or limited access to radiological expertise, particularly in primary care clinics, there is an urgent need to establish a standardized, objective, and automated diagnostic support system to improve diagnostic efficiency and consistency.

Recent deep learning models have demonstrated high reliability in accurately analyzing various implant features and patterns on PAs, achieving over 95 % classification accuracy in implant identification tasks. [27–30] However, to our knowledge, no comprehensive studies have addressed AI-assisted evaluation of peri-implant conditions. In 2022, Liu et al. proposed an initial peri-implant classification approach using a Faster R–CNN–based detection model,[21] reporting an accuracy of 81 % and specificity of 87 %, though without assessing its clinical applicability. Subsequently, in 2023, Chen et al. built upon this foundation by integrating image processing techniques, improving peri-implant detection efficiency.[30] Their method combined YOLOv2 with image enhancement, achieving a classification accuracy of 97.5 %, representing a 16.1 % improvement over models without image processing. Nevertheless, both studies primarily focused on identifying potential peri-implant cases rather than quantifying the extent of bone loss or assigning severity levels. To address this, Lee et al., in 2024 attempted to distinguish between "bone loss" and "non-bone loss" conditions using YOLOv7, calculating the bone loss ratio based on the bounding box height.[31] However, this method presented two key limitations: first, the bounding box height defined by the AI model lacked consistency, resulting in variation across repeated inferences; second, the assessment of peri-implant severity remained a manual task, failing to achieve full automation and still imposing a partial burden on clinical practice.

In contrast, our study aimed to address the limitations encountered by previous state-of-the-art methods. By integrating YOLO-based localization for precise peri-implant detection, our system achieved an accuracy of 98.7 % and a precision of 98.1 %, representing a 1.2 %

Table 3 Comparison of validation results with ground truth for bone loss severity.

Grade level	Ground truth and validate result			
Grade A	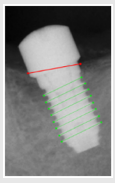	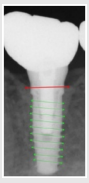	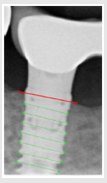	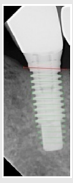
Framework accuracy/inference time	95.93 %/0.21s	97.45 %/0.13s	96.71 %/0.17s	96.12 %/0.23s
Manual evaluation accuracy/interpretation time	89.32 %/3s	85.73 %/6s	93.51 %/5s	92.37 %/9s
Grade B		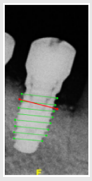	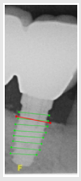	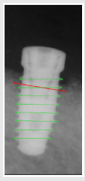
Framework accuracy/inference time	95.64 %/0.22s	96.92 %/0.12s	96.44 %/0.27s	96.09 %/0.16s
Manual evaluation accuracy/interpretation time	95.12 %/5s	90.18 %/8s	88.24 %/10s	89.44 %/7s
Grade C	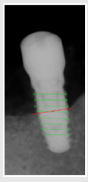	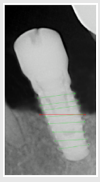	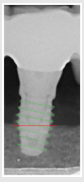	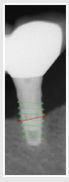
Framework accuracy/inference time	95.12 %/0.18s	97.11 %/0.19s	99.264 %/0.15s	98.18 %/0.13s
Manual evaluation accuracy/interpretation time	91.12 %/9s	86.32 %/6s	88.33 %/8s	93.33 %/6s

Grade A: no bone loss with bone loss percentage less than 25 %. Grade B: indicated moderate bone loss with 25 % to less than 50 % loss. Grade C: represented severe bone loss with 50 % or more.

improvement over prior studies.[30] Furthermore, we established the ALC as the baseline for evaluating bone loss severity. We developed an image-processing-based algorithm to classify the severity of peri-implant bone loss. The key contributions and innovations of this study are summarized as follows:

1. We proposed a fully automated assessment system for peri-implantitis severity, categorizing peri-implant bone loss into three grades. Our framework achieved classification accuracy of 96.61 % for Grade A, 95.00 % for Grade B, and 95.18 % for Grade C, with an overall accuracy of 95.8 %.
2. Clinical validation was conducted by comparing the system's predictions with dental expert annotations. The results demonstrated that the proposed system could operate approximately 36 times faster than manual interpretation and improve diagnostic accuracy for severity classification by about 7.5 %.

However, this study has several limitations. The classification of peri-implantitis severity was based on the 2018 staging system, which in our current framework allows for only three levels of severity. Based on our experimental findings, cases with less than 25 % bone loss should ideally be subdivided into two categories: bone loss $<$15 % of implant length and 15 %—25 % of implant length. Our model struggled to accurately classify cases in the 15 % range, leading to decreased classification performance, with an accuracy of only approximately 84.23 %. In addition, we tested the model under suboptimal image quality conditions, such as excessively blurred implant regions or images with extreme brightness or darkness. The classification accuracy declined to approximately 78.12 %—84.89 % (95 % CI 70.31 %—87.26 %), accompanied by a noticeable reduction in model confidence scores. In future work, we aim to incorporate image enhancement and quality normalization techniques to mitigate the impact of suboptimal imaging conditions.

Moreover, the dataset used in this study was derived exclusively from the PA image database of the Chang Gung Medical Foundation in Taiwan, limiting the generalizability of our findings to populations with different oral characteristics. Additionally, our system is designed to serve as an auxiliary diagnostic tool. To ensure accuracy, a more comprehensive diagnosis of peri-implant conditions should incorporate additional imaging modalities, such as CT. We encourage future research to refine the classification

granularity and to incorporate PA datasets from diverse geographic populations for broader training and evaluation.

In conclusion, the integration of artificial intelligence and image processing techniques has been validated in this study as a practical approach to assess the severity of peri-implant bone loss. The proposed system demonstrated promising clinical outcomes, offering reliable assistance for experienced dental professionals during diagnosis and as a potential training tool for novice dentists. This research contributes to the advancement of automated diagnostic technologies in clinical dentistry and underscores the practical value of AI-assisted tools in enhancing diagnostic accuracy and efficiency.

Declaration of competing interest

The authors have no conflicts of interest relevant to this article.

Algorithm 1. Implant image rotation.

Input: I: Binary image with implant contour
Output: I_r: Rotated image, θ: Rotation angle
1: contours = Get_all_Outline(I)
2: C_{main} = Largest_outline (contours)
3: (center_point, (width, height), $\theta_{Original}$) = Min_area_box (C_{main})
4: **if** arctan ($\theta_{Original}$) < 45° **then**
5: $\theta = 90 + \theta_{Original}$
6: else
7: $\theta = \theta_{Original}$
8: I_r = Rotate_Image (I, θ)
9: **return** I_r, θ

Acknowledgments

This work was supported by the National Science and Technology Council (NSTC), Taiwan, under grant numbers of NSTC-112-2410-H-033-014. This work involved human subjects or animals in its research. Approval of all ethical and experimental procedures and protocols was granted by the Research Institution Review Board (IRB) under Application No. 202500009B0.

References

1. Dung SZ. A novel combined implantoplasty and regenerative surgical approach to salvage implants: a report on two 20-year-old implants. *J Dent Sci* 2025;20:1993–5.
2. Diaz P, Gonzalo E, Villagra LJG, Miegimolle B, Suarez MJ. What is the prevalence of peri-implantitis? a systematic review and meta-analysis. *BMC Oral Health* 2022;22:449.
3. Hwang S, Lee HM, Yun PY, Kim YK. Survival analysis of implants after surgical treatment of peri-implantitis based on bone loss severity and surgical technique: a retrospective study. *BMC Oral Health* 2023;23:308.
4. Monje A, Amerio E, Farina R, et al. Significance of probing for monitoring peri-implant diseases. *Int J Oral Implant* 2021;14:385–99.
5. Elemek E, Agrali OB, Kuru B, Kuru L. Peri-implantitis and severity level. *Eur J Dermatol* 2020;14:24–30.
6. Tonetti MS, Greenwell H, Kornman KS. Staging and grading of periodontitis: framework and proposal of a new classification and case definition. *J Clin Periodontol* 2018;45:S149–61.
7. Sanz M, Dahlin C, Apatzidou D, et al. Biomaterials and regenerative technologies used in bone regeneration in the craniomaxillofacial region: consensus report of group 2 of the 15th European workshop on periodontology on bone regeneration. *J Clin Periodontol* 2019;46:82–91.
8. Silveira-Neto N, Flores ME, De Carli JP, et al. Peri-implant assessment via cone beam computed tomography and digital periapical radiography: an ex vivo study. *Clinics* 2017;72:708–13.
9. Aggarwal R, Sounderajah V, Martin G, et al. Diagnostic accuracy of deep learning in medical imaging: a systematic review and meta-analysis. *npj Digit Med* 2021;4:65.
10. Putra RH, Doi C, Yoda N, Astuti ER, Sasaki K. Current applications and development of artificial intelligence for digital dental radiography. *Dentomaxillofacial Radiol* 2022;51:20210197.
11. Khanagar SB, Al-ehaideb A, Maganur PC, et al. Developments, application, and performance of artificial intelligence in dentistry – a systematic review. *J Dent Sci* 2021;16:508–22.
12. Liu J, Liu X, Shao Y, et al. Periapical lesion detection in periapical radiographs using the latest convolutional neural network ConvNeXt and its integrated models. *Sci Rep* 2024;14:25429.
13. Dashti M, Londono J, Ghasemi S, et al. Evaluation of accuracy of deep learning and conventional neural network algorithms in detection of dental implant type using intraoral radiographic images: a systematic review and meta-analysis. *J Prosthet Dent* 2025;133:137–46.
14. Park JH, Moon HS, Jung HI, Hwang J, Choi YH, Kim JE. Deep learning and clustering approaches for dental implant size classification based on periapical radiographs. *Sci Rep* 2023;13:16856.
15. Oh S, Kim YJ, Kim J, et al. Deep learning-based prediction of osseointegration for dental implant using plain radiography. *BMC Oral Health* 2023;23:208.
16. Lee JH, Kim YT, Lee JB. Identification of dental implant systems from low-quality and distorted dental radiographs using AI trained on a large multi-center dataset. *Sci Rep* 2024;14:12606.
17. Lee JH, Jeong SN. Efficacy of deep convolutional neural network algorithm for the identification and classification of dental implant systems, using panoramic and periapical radiographs: a pilot study. *Medicine* 2020;99:e20787.
18. Bennani S, Regnard NE, Ventre J, et al. Using AI to improve radiologist performance in detection of abnormalities on chest radiographs. *Radiology* 2023;309:e230860.
19. Mameno T, Wada M, Nozaki K, et al. Predictive modeling for peri-implantitis by using machine learning techniques. *Sci Rep* 2021;11:11090.
20. Fransson C, Tomasi C, Pikner SS, et al. Severity and pattern of peri-implantitis-associated bone loss. *J Clin Periodontol* 2010;37:442–8.
21. Liu M, Wang S, Chen H, Liu Y. A pilot study of a deep learning approach to detect marginal bone loss around implants. *BMC Oral Health* 2022;22:11.
22. Atieh MA, Alsabeeha NHM, Faggion JrCM, Duncan WJ. The frequency of peri-implant diseases: a systematic review and meta-analysis. *J Periodontol* 2013;84:1586–98.
23. Sanz-Sánchez I, Ortiz-Vigón A, Sanz-Martín I, Figuero E, Sanz M. Effectiveness of lateral bone augmentation on the alveolar crest dimension: a systematic review and meta-analysis. *J Dent Res* 2015;94:128S–42S.

24. Buonocunto N, Cinquini C, Mijiritsky E, et al. Effect of alveolar ridge preservation on peri-implant mucositis and peri-implantitis prevalence: a multicenter, cross-sectional study. *Clin Implant Dent Relat Res* 2023;25:1044—55.
25. Qahash M, Susin C, Polimeni G, Hall J, Wikesjö UME. Bone healing dynamics at buccal peri-implant sites. *Clin Oral Implants Res* 2008;19:166—72.
26. Schwarz F, Derks J, Monje A, Wang HL. Peri-implantitis. *J Clin Periodontol* 2018;45:S246—66.
27. Kim HS, Ha EG, Kim YH, Jeon KJ, Lee C, Han SS. Transfer learning in a deep convolutional neural network for implant fixture classification: a pilot study. *Imaging Sci Dent* 2022;52:219—24.
28. Kong HJ. Classification of dental implant systems using cloud-based deep learning algorithm: an experimental study. *J Yeungnam Med Sci* 2023;40:S29—36.
29. Hsiao CY, Bai Hexin, Ling Haibin, Yang Jie. Artificial intelligence in identifying dental implant systems on radiographs. *Int J Periodontics Restor Dent* 2023;43:363—8.
30. Chen YC, Chen MY, Chen TY, et al. Improving dental implant outcomes: CNN-based system accurately measures degree of peri-implantitis damage on periapical film. *Bioengineering* 2023;10:640.
31. Lee WF, Day MY, Fang CY, et al. Establishing a novel deep learning model for detecting peri-implantitis. *J Dent Sci* 2024;19:1165—73.